WORLD CONFERENCE ON TIMBER ENGINEERING 2025
BRISBANE, AUSTRALIA

Advancing Timber for the Future Built Environment

EXPERIMENTAL STUDY ON SEISMIC RETROFIT USING SEISMIC RESPONSE CONTROL DEVICES IN A TEMPLE

Suzuki Hokuto[1], Okada Yuka[2], Kajikawa Hisamitsu[3]

ABSTRACT: In Japan, temples typically have extremely heavy roofs and roof frames, and because there are few existing mad walls or wood lathing walls, their overall seismic performance tends to be very low due to insufficient stiffness. In this study, as a seismic retrofit method for such temples, we have proposed and developed a reinforcement system using seismic response control devices with high-damping rubber. This system improves strength, stiffness, and damping performance without altering the building's layout, interior, or exterior appearance. A horizontal loading test was conducted to investigate the structural characteristics of the reinforced structure and to examine how variations in parameters affect these characteristics. Furthermore, a mechanical model was proposed, and by decomposing the experimental results based on deformation mode theory, it was confirmed that the seismic response control devices worked effectively as reinforcement.

KEYWORDS: seismic retrofit, seismic response control device, high-damping rubber, horizontal loading test, temple

1 – INTRODUCTION

Currently, there are approximately 76,000 temples remaining in Japan, and these structures have long served as spiritual centers, places for community interaction, and hubs of education and culture, deeply connected to local societies. A temple photograph is shown in Figure 1. On the other hand, it has been reported that the damage rate of temples tends to be high during large earthquakes. The reasons for this include the following: temples generally have a large and heavy roof. Additionally, the seismic elements mainly consist of frameworks with tie rods and bearing walls (such as mad walls and wood lathing walls), all of which have low stiffness and strength. Moreover, in terms of bearing walls, the amount is often insufficient, and their placement tends to be eccentric, leading to a significant reduction in overall seismic performance.

In addition, temples that are not designated as national treasures or cultural properties rely on funding from parishioners, which is inherently limited. Under these circumstances, it is urgently necessary to develop an effective seismic retrofit method for such temples, which can improve both stiffness and strength without altering the layout, while also enhancing damping performance.

Therefore, this study proposes a seismic response control device reinforcement method in which large columns are mutually connected using seismic response control devices made of high-damping rubber with frictional properties. This method aims to improve the stiffness, strength, ductility, and damping—the key hysteresis characteristics of a temple—and to raise the structural performance to a level that meets the design standards of the current Building Standards Act and the Act on the Promotion of Housing Quality Assurance through seismic retrofit.

First, a horizontal loading test is conducted on the seismic response control device reinforcement to clarify its loading-displacement relationship, reference skeleton curve, equivalent stiffness, hysteresis area, and equivalent viscous damping factor. Then, a mechanical model for the seismic response control device reinforcement is proposed, and experimental values are analyzed using this model.

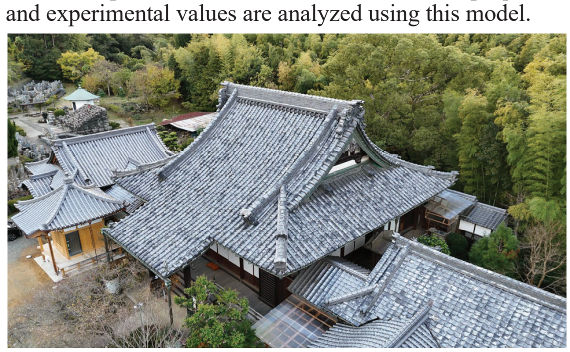

Figure 1. Temple

[1] Hokuto Suzuki, Meiji Univ, Graduate Student, Tokyo, Japan, Lingmub511@gmail.com

[2] Yuka Okada, MisawaHomes Institute of Research and Development Co.Ltd., M.Eng., Tokyo, Japan, Yuka_Okada@home misawa.co.jp

[3] Hisamitsu Kajikawa, Meiji Univ, Prof, Dr.Eng., Tokyo, Japan, kajihisa@meiji.ac.jp

https://doi.org/10.52202/080513-0492

2 – HORIZONTAL LOADING TEST OF SEISMIC RESPONSE CONTROL DEVICES

2.1 OVERVIEW OF SEISMIC RESPONSE CONTROL DEVICES

The seismic response control device is fundamentally designed to be installed between columns. This makes it applicable at any position within the span, as long as it is located between columns. Possible positions include the column base, the column head, and within walls, which makes it particularly well-suited for application to temples where bearing walls are limited. An example of reinforcement using the seismic response control device is shown in Figure 2.

The mechanism of the seismic response control device connects columns with a tie member, with the frame and center panel joined by a center pin. A high-damping rubber damper is attached to the tip of the center panel. A schematic view of the seismic response control device incorporating high-damping rubber is shown in Figure 3.

When a column tilts, the tie member and frame move together, causing the center pin to move vertically. This in turn, causes the center panel to incline significantly, resulting in a large deformation of the high-damping rubber damper.

This mechanism effectively amplifies the deformation of the high-damping rubber damper in response to the relative story displacement of the building, enabling it to function efficiently.

2.2 OVERVIEW OF TEST SPECIMEN

Figure 4 is shown in the schematic of the test specimen. The test specimen used in this experiment partially replicates the framework that forms the wall of a typical temple building. The width of the specimen uses the actual dimensions of the temple (2,181 mm), and the height was set to be as close as possible to the actual dimensions (3,120 mm) while accommodating the jig and excitation device. The specimen was designed with the assumption of reinforcing the floor, with a seismic response control device incorporating high-damping rubber installed between the column bases. One of the columns is fixed to the deformation amplification mechanism, while the other column is fixed and bolted together between them. In this detail, the pin spacing, column spacing, and column height were adjusted to control the amplification rate of the deformation mechanism. The rubber deformation is expected to be approximately 60 mm when the temple undergoes a deformation of about 1/100 rad. The high-damping rubber used in this device is manufactured by Sumitomo Rubber Industries, Ltd. It has high stiffness, strength, ductility, and damping performance, and when combined with the deformation amplification mechanism, it can effectively control the relationship between the building's relative story displacement and the high-damping rubber. This allows the creation of effective restoration characteristics for temple architecture. Additionally, since the purpose of this experiment is to evaluate the performance of the seismic response control device, an experimental column, covered with glued laminated timber over an H-shaped steel frame, was used to prevent premature failure of the column.

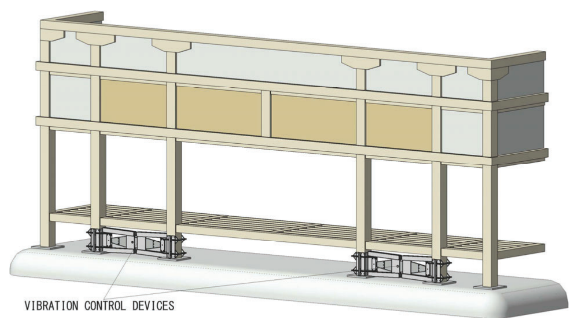

Figure 2. Concept of Reinforcement Using a Seismic Response Control Device

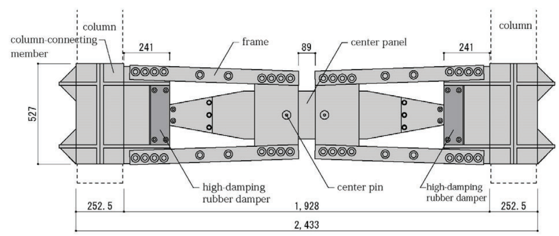

Figure 3. Schematic view of the seismic response control device

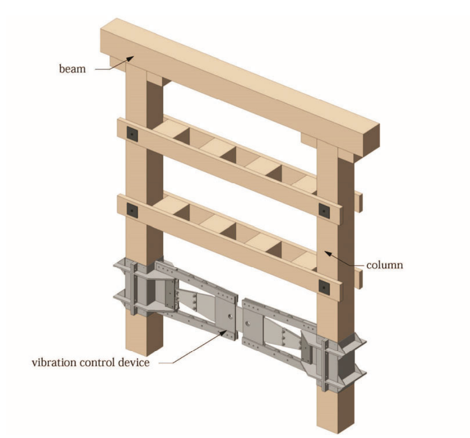

Figure 4. Schematic of test specimen

https://doi.org/10.52202/080513-0492

The test specimen name is shown in Figure 5, with the size, thickness, type of high-damping rubber, and the frame of the seismic response control device as the parameters.

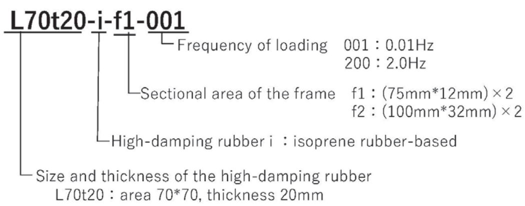

Figure 5. Test specimen name and parameters

2.3 OVERVIEW OF TEST

The experimental overview is shown in Figure 6. To reproduce the structural characteristics of actual temple architecture, in which the base of each column is prevented from lifting due to the weight of the roof and roof framing, the column bases were not fixed and a tie rod system was employed. Vibrations were applied using a 200 kN actuator. To ensure that the tie rods did not obstruct horizontal excitation, steel plates, rollers, and steel plates were sequentially stacked at the positions corresponding to the tops of the columns of the test specimen. Tie Rod Girder 1 and Tie Rod Girder 2 were placed on top of these, and the frame and Tie Rod Girder 2 were connected with (PC steel rods). In addition, stoppers were installed to restrain horizontal displacement at the column bases in the direction of excitation.

In L70t20-i-f1, stoppers were placed both inside and outside the column bases on both sides, creating a situation in which each column base had its own support point. In contrast, in L70t20-i-f2, stoppers were installed only on the outside of the columns, and glued laminated timber was inserted on the inside. As a result, the support point was limited to the outside of one of the columns.

Vibrations were applied by pushing and pulling a horizontal loading jig attached to a loading girder using a 200 kN actuator installed on a reaction wall. Since the column bases were not fixed and a tie rod system was used, a vertical load of approximately 40 kN was applied to each column by tensioning four prestressing steel rods to approximately 20 kN each prior to excitation, after which horizontal excitation was performed.

The loading schedule involved applying four repeated positive and negative excitations alternately while controlling the apparent story deformation angle to reach values of ±1/600, ±1/450, ±1/300, ±1/200, ±1/150, ±1/100, ±1/75, ±1/50, and ±1/30 [rad]. Excitation was performed at vibration frequencies of 0.01 Hz and 2.0 Hz, within a deformation angle range of either ±200% or ±400% relative to the thickness of the high-damping rubber. The combinations of excitation frequency and deformation angle are shown in Table 1, where "◯" indicates that a test was conducted, and "–" indicates that it was not.

Although L70t20-i-f2-0.01 was scheduled to be performed up to a deformation angle of 1/30 [rad], the test was terminated at 1/50 [rad] due to instability in the apparatus.

The relationship between the load acting on the tie rods (prestressing steel rods) and the story deformation angle is shown in Figure 7. The load acting on the tie rods was calculated from strain gauges attached to the prestressing steel rods, using the average values of the two rods on the right and the two on the left sides of the test specimen. The reason for the larger difference between the left and right

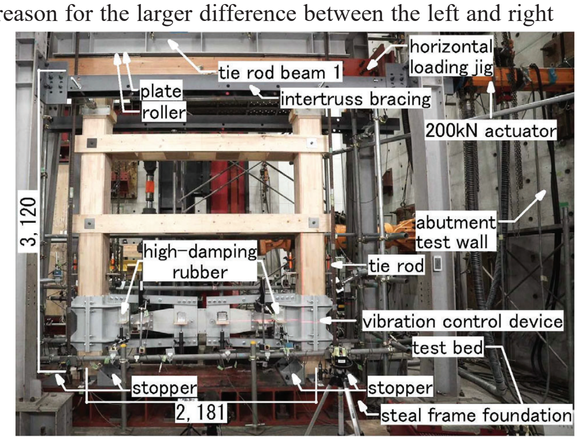

Figure 6. Experimental setup diagram

Table 1. Loading status

Name	Frequency	Apparent shear deformation								
		±1/600	±1/450	±1/300	±1/200	±1/150	±1/100	±1/75	±1/50	±1/30
L70t20-i-f1	0.01Hz	◯	◯	◯	◯	◯	◯	◯	◯	◯
	2.0Hz	◯	◯	◯	◯	◯	◯	◯	◯	◯
L70t20-i-f2	0.01Hz	◯	◯	◯	◯	◯	◯	◯	◯	-
	2.0Hz	◯	◯	◯	◯	◯	◯	◯	◯	◯

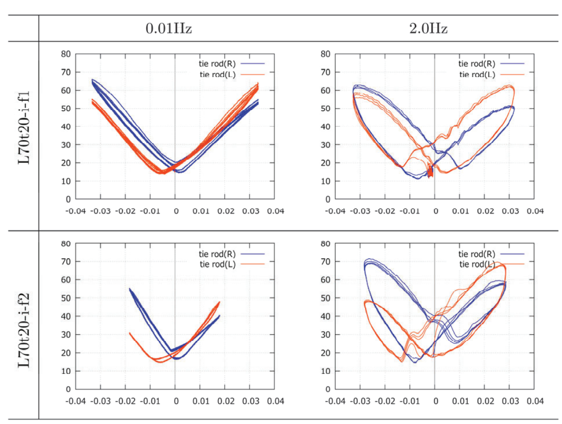

Figure 7. Loading-displacement relationship of the tie rod (vertical axis: load [kN], horizontal axis: story deformation angle [rad])

https://doi.org/10.52202/080513-0492

tie rods in L70t20-i-f2 is considered to be the influence of overall rotational deformation resulting from differences in the column base support conditions.

3. RESULTS OF TEST

The experimental results for each test specimen up to a story deformation angle of 1/30 [rad] are shown. Since L70t20-i-f2 was subjected to horizontal loading up to 1/50 [rad], the figures up to 1/50 [rad] are presented.

The loading–displacement relationships for each test specimen are shown in Figure 8. The load applied to the test specimen was obtained by subtracting the inertial force of the test specimen from the actuator load. The inertial force was calculated by multiplying the acceleration at the center of the loading beam by the mass of the upper half of the test specimen, considering the height from the steel frame foundation to the center of the loading beam (3,120 [mm]) as the height of the column. The story deformation angle was calculated by dividing the relative story displacement, obtained by subtracting the horizontal displacement of the column base from the displacement of the loading beam, by the specimen height of 3,120 [mm].

All test specimens exhibited spindle-shaped hysteresis loops, indicating high damping performance. This behavior is considered to be due to the large hysteresis areas resulting from the damping performance of the high-damping rubber, the plastic deformation of the seismic response control device frame, and the friction at the joints. It should be noted that no specimen failed at 1/30 [rad], and the maximum load was not reached.

The skeleton curves, equivalent stiffness, hysteresis areas, and equivalent viscous damping ratios are shown in Figure 9. In all figures, the horizontal axis represents the story deformation angle [rad]. Comparing the loading–displacement relationships on the skeleton curves, in terms of frame differences, L70t20-i-f2-200 (85.0 kN) exhibited a load approximately 1.3 times greater than that of L70t20-i-f1-200 (66.6 kN) at 1/50 [rad]. Although differences due to loading frequency were not significant, values at 2.0 [Hz] tended to be slightly higher than those at 0.01 [Hz] in the range of 1/200–1/75 [rad]. The equivalent stiffness exhibited the same trend as the skeleton curves.

When comparing the hysteresis areas, in terms of frame differences, L70t20-i-f2-200 (1.97 kN·rad) was approximately 1.4 times larger than L70t20-i-f1-200 (1.41 kN·rad) at 1/50 [rad]. Regarding loading frequency, at 1/50 [rad], L70t20-i-f1-200 (1.41 kN·rad) showed a value approximately 1.4 times larger than L70t20-i-f1-001 (1.00 kN·rad).

Comparing the equivalent viscous damping ratios, for the test specimen at a loading frequency of 2.0 [Hz], values were approximately 5–8% around 1/200 [rad], and approximately 15–18% around 1/50 [rad]. These results are attributed to the balance achieved by the serial combination of friction at the frame joints, the plasticity of the frame, and the damping performance of the high-damping rubber.

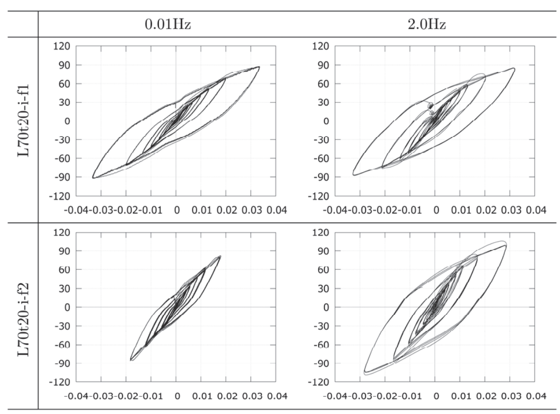

Figure 8. Loading-displacement relationship (vertical axis: load [kN], horizontal axis: story deformation angle [rad])

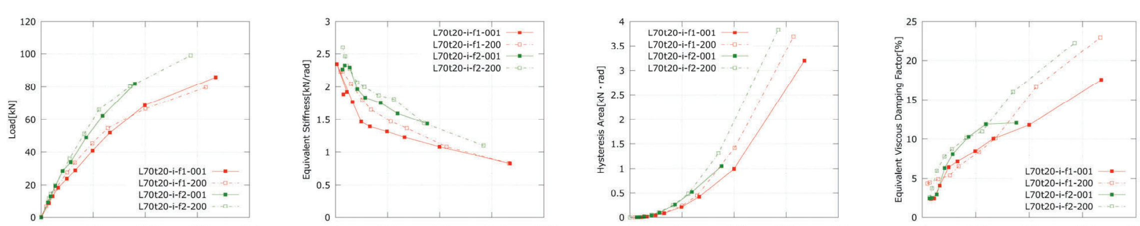

Reference Skeleton Curve | Equivalent Stiffness | Hysteresis Area | Equivalent Viscous Damping Factor

Figure 9. Results

4. DEFORMATION MODE THEORY

The concept of the deformation mode theory for reinforcement using seismic response control devices is shown in Figure 10. When subjected to a horizontal load P [kN], the overall deformation δ can be theoretically derived by summing the following deformation modes: the shear deformation mode of the high-damping rubber in the seismic response control device (high-damping rubber deformation mode) δ_D, the column bending deformation mode δ_B, the deformation mode due to the plastic deformation of the frame of the seismic response control device (frame deformation mode) δ_{FF}, and the deformation mode due to friction at the joints (frame joint deformation mode) δ_{FR}.

Here, L is the distance between the centers of the columns, h is the specimen height, h_1 is the height from the column base to the top end of the seismic response control device, and h_2 is the height from the column top to the top end of the seismic response control device. The relationships between displacement and load for each deformation mode are expressed in Equations (1) to (5).

Overall deformation δ

$$\delta = \delta_D + \delta_B + \delta_{FF} + \delta_{FR} \tag{1}$$

High-damping rubber deformation mode δ_D

The relationship between δ_D and P is given by Equation (2), based on the equilibrium of force moments and the equilibrium of energy.

$$\delta_D = \frac{{L_c}^2 h^2}{2(L_s + L_c)^2 \times {L_g}^2 \times G_{ge}} \times P \tag{2}$$

L_c : Distance Between Pins of the Seismic Control Device

L_s : distance from pins to the inside of the column

L_g : distance from pins at the center of the high damping rubber

G_g : shear Modulus of High Damping Rubber

Column bending deformation mode δ_B

The relationship between δ_B and P is given by Equation (3), based on the cantilever beam formula.

$$\delta_B = \frac{P{h_1}^2}{6EI} \tag{3}$$

Frame deformation mode δ_{FF}

The relationship between δ_{FF} and P is given by Equation (4), based on the cantilever beam formula and the law of the conservation of energy.

$$\delta_{FF} = \frac{{L_f}^3}{6EI}\left\{\frac{(2L_g + L_c)h}{(2L_s + L_c)L_g}\right\}^2 \times P \tag{4}$$

L_f : frame length

Frame joint deformation mode δ_{FR}

The relationship between δ_{FF} and P is given by Equation (5), based on Hooke's law and the law of the conservation of energy.

$$\delta_{FR} = \frac{1}{2R_f}\left\{\frac{L_f(2L_g + L_c)h}{(2L_s + L_c)L_g}\right\}^2 \times P \tag{5}$$

P' : force on pins

R_f : rotational stiffness of frame friction hinges

θ_f : rotation angle of frame joint

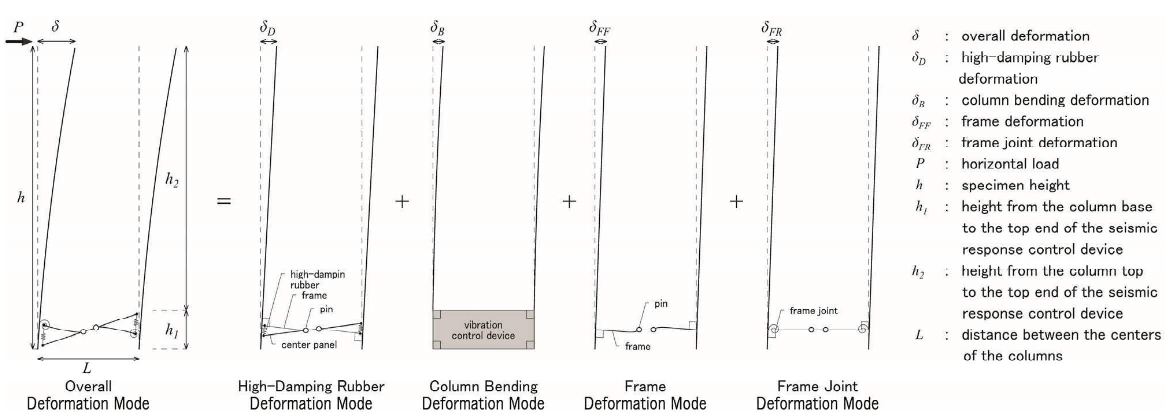

Figure 10. Concept of the deformation mode theory

https://doi.org/10.52202/080513-0492

5 . EXPERIMENTAL DATA DECOMPOSITION BACED ON DEFORMATION MODE THEORY

5.1 DECOMPOSITION METHOD

The experimental results for the loading–displacement relationship, reference skeleton curve, and hysteresis area were decomposed by each deformation mode, and the experimental values were examined.

The arrangement of the measuring devices used for this decomposition is shown in Figure 11. This arrangement was the same for all test specimens.

The total deformation δ was taken from the experimental values, while the deformation of the high-damping rubber δ_D, was obtained using a theoretical equation.

The deformation of the high-damping rubber damper δ_g was calculated by converting the experimentally measured data (19ch, 20ch) into the true deformation values of the high-damping rubber damper (19ch', 20ch'), and these converted values were input into the calculation.

The bending deformation of the columns δ_B was also obtained using a theoretical equation, where *EI* was calculated from the experimental values and approximated as a linear relationship.

This approximation equation is shown below, and the experimental values were used as the input for the load *P* [kN] and displacement *x* [rad].

As for the deformation modes of the frame, since it was difficult to separate the experimental values into δ_{FF} and δ_{FR}, the total frame deformation was taken as $\delta_F = \delta_{FF} + \delta_{FR}$, and it was calculated as δ_F by subtracting the deformation of the high-damping rubber δ_D and the column bending deformation δ_B from the total deformation δ.

The deformation modes for the reference skeleton curve were evaluated using the maximum load and the relative story displacement at the first loading loop.

The deformation modes for the hysteresis area were evaluated using the results from the third loading loop, and the hysteresis areas at the maximum deformation for the high-damping rubber deformation δ_D, the column bending deformation δ_B, and the total frame deformation δ_F ($\delta_{FF} + \delta_{FR}$) were calculated and plotted.

5.2 DECOMPOSITION RESULTS

The loading–displacement relationships for each deformation mode are shown in Figure 12. The total deformation δ is shown in green, the deformation mode of the high-damping rubber δ_D in blue, the bending deformation mode of the columns δ_B in orange, and the frame deformation mode δ_F in red.

For specimen L70t20-i-f2-001, the test was interrupted at 1/50 [rad] due to a malfunction of the test apparatus, resulting in different behavior compared to the other specimens. At this stage, the safety mechanism had not yet been activated, and δ_D exhibited a large hysteresis, whereas δ_F remained linear without any hysteresis loop. The same trend was observed in the other test specimens.

In contrast, for all other specimens (at 1/30 [rad]), δ_F exhibited a large hysteresis loop, which indicates that δ_F underwent plastic deformation as the preset safety limit load was approached, causing the safety mechanism to be activated.

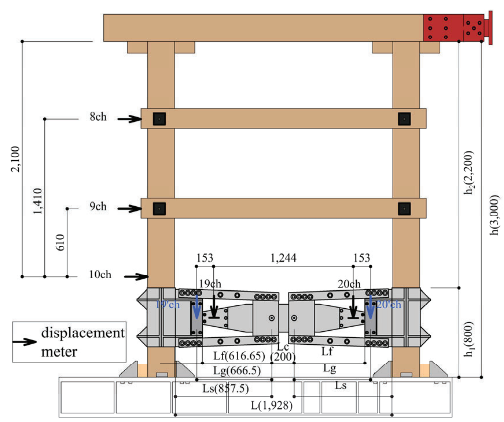

Figure 11. Arrangement of measuring devices

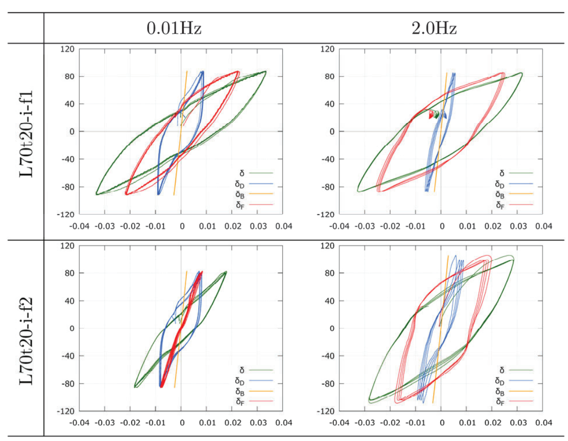

Figure 12. Loading-displacement relationship for each deformation mode (vertical axis: load [kN], horizontal axis: story deformation angle [rad])

The results of the decomposition of the reference skeleton curves are shown in Figure 13.

For L70t20-i-f1, at 0.01 [Hz], the deformation mode of the high-damping rubber δ_D remained very small within the small story deformation angle range, and the total deformation δ started to increase around 1/250 [rad]. At 2.0 [Hz], it remained small until around 1/100 [rad]. For L70t20-i-f2, both at 0.01 [Hz], δ_D remained very small in the small deformation range and began to increase around 1/300 [rad]. Around 1/100 [rad], δ_F was approximately 1.5 times greater than δ_D, and the excitation frequency had little influence on this behavior.

The results of the hysteresis area decomposition are shown in Figure 14.

Except for L70t20-i-f2-001, the total frame deformation δ_F accounted for the largest proportion among the test specimens. The bending deformation mode of the columns δ_B was very small, regardless of the frame type or excitation frequency. For L70t20-i-f2, by increasing the cross-sectional area of the seismic response control device frame, it was possible to suppress the frame deformation δ_{FF}, and the proportion of the total frame deformation δ_F to the total deformation δ became slightly smaller compared to L70t20-i-f1.

From these results, it can be considered that the strength and damping performance of the seismic response control device reinforcement is attributed to the fact that δ_D and the total frame deformation mode δ_F (consisting of the frame deformation mode δ_{FF} and the frame joint deformation mode δ_{FR}) are connected in series.

6– CONCLUSION

The structural characteristics were clarified through horizontal loading tests of the seismic response control device reinforcement. In addition, the effects of differences in frame type and loading frequency on the structural characteristics were investigated. Furthermore, a mechanical model was proposed, and by applying it to decompose the experimental values, it was confirmed that the seismic response control device reinforcement functioned effectively.

7 – REFERENCES

[1] Hisamitsu Kajikawa: Experimental verification of seismic device performance through mutual bonds of large columns in temples, 2022 Matsui Kakuhira Memorial Foundation Experimental Report, June 2024.

[2] Yuna Igarashi, Hisamitsu Kajikawa, Haruhiko Ogawa, Mayuko Takaoka, Chongbing Yan: Experimental study on the mechanical properties of high-damping rubber dampers, Japan Earthquake Engineering Symposium, G419-21, November 2023.

[3] Hisamitsu Kajikawa, Yuka Okada: Horizontal excitation test of vibration control device reinforcement through mutual bonds of large cross-section columns in temple architecture – Part 1: Development objectives, overview of vibration control device reinforcement, and horizontal excitation test, JAEE Conference, December 2024.

[4] Yuka Okada, Hisamitsu Kajikawa: Horizontal excitation test of vibration control device reinforcement through mutual bonds of large cross-section columns in temple architecture – Part 2: Development of deformation modal theory and mechanical model, JAEE Conference, December 2024.

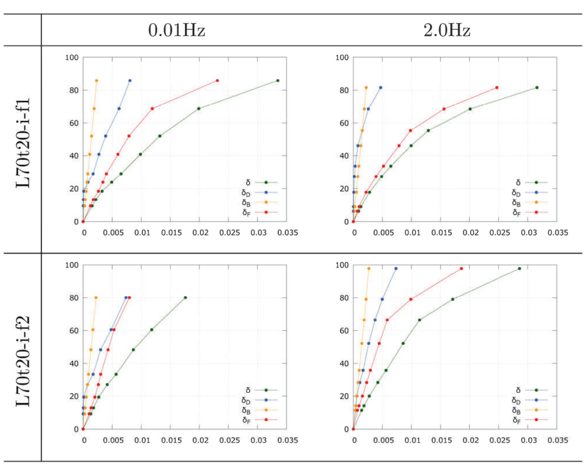

Figure 13. reference skeleton curves for each deformation mode (vertical axis: load [kN], horizontal axis: story deformation angle [rad])

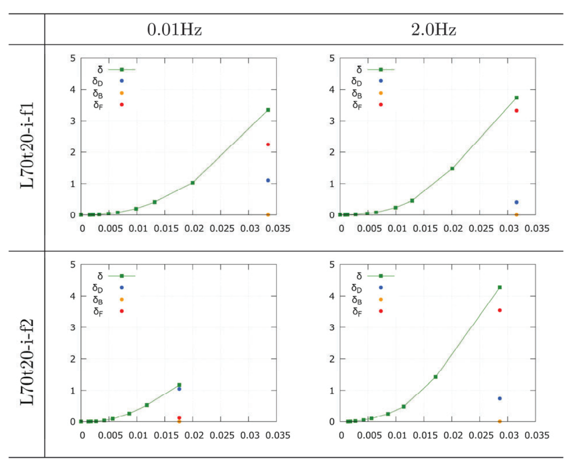

Figure 13. hysteresis area for each deformation mode (vertical axis: load [kN], horizontal axis: story deformation angle [rad])

https://doi.org/10.52202/080513-0492